Journal of Power Sources 196 (2011) 5349–5356

Contents lists available at ScienceDirect

Journal of Power Sources

journal homepage: www.elsevier.com/locate/jpowsour

Characterization of high-power lithium-ion batteries by electrochemical impedance spectroscopy. II: Modelling

D. Andre[a,*], M. Meiler[a], K. Steiner[a], H. Walz[a], T. Soczka-Guth[a], D.U. Sauer[b]

[a] Deutsche ACCUmotive GmbH & Co. KG, Neue Str. 95, D-73230 Kirchheim/teck, Germany
[b] Rheinisch Westfälische Technische Hochschule Aachen, Jägerstr. 17, D-52066 Aachen, Germany

ARTICLE INFO

Article history:
Received 15 June 2010
Received in revised form 16 July 2010
Accepted 25 July 2010
Available online 3 August 2010

Keywords:
Lithium-ion batteries
Electrochemical impedance spectroscopy
Equivalent circuit models

ABSTRACT

A common way to model lithium-ion batteries is to apply equivalent circuit (EC) models. In this work two different EC models are build up and parameterized for a commercial 6.5 Ah high-power lithium-ion cell. Measured impedance spectroscopy data depending on temperature and state of charge (SOC) are used for parameter estimation.

The first EC model consists of an ohmic resistor (R), an inductor (L) and three RC-elements (a parallel connection of a capacitor (C) and a resistor). The second EC model consists of one R, one L, two Zarc elements and a Warburg element. The estimated parameters were used to develop two empirical electrical cell models which are able to predict the voltage of the cells depending on current, temperature and SOC. Hereby the internal cell resistance Ri is based on the EC models and a Butler–Volmer adjustment. Both approaches were validated by current profiles, which cover typical automotive applications to prove the model performance at low temperatures and high dynamic operation. An accurate voltage prediction could be realized with both EC models. The second, more complex, model is able to predict cell voltage more precisely, but at the expense of up to four times higher computational effort.

1. Introduction

In order to predict the performance of a battery cell depending on operation conditions and load, simulations based on an equivalent circuit (EC) model are widely used [1,2]. In this work two EC models with different complexities are presented and compared in terms of simulation performance and effort. The generalized method to identify these models is presented in Fig. 1.

In the first step the parameters of the model have to be estimated. Therefore impedance spectra gained by the EC are fitted to experimental measured data through a numerical optimization. Afterwards the estimated parameters are implemented into a cell model. Finally, the model is validated by comparison to measured data.

A precise prediction of voltage allows testing battery cells under different conditions just by simulation and therefore reduces experimental efforts and time. Moreover simulations allow an optimization of the battery and in the next step of drive trains for upcoming hybrid and electrical vehicles.

In a previous work [3] impedance spectra were recorded for a high-power 6.5 Ah lithium-ion cell in a temperature range from −30 °C to 50 °C for the entire state of charge (SOC) range. These spectra contain all information about cell impedance depending on operating conditions and allow therefore a prediction of the cell performance under different loads and scenarios. Based on these spectra both EC models are set, verified, validated and compared in terms of computation time and accuracy of voltage prediction.

2. Theory

2.1. Equivalent circuit with RC-elements

The first applied EC to model cell voltage was built up in a most simple way in order to have a basic model. Aim of this approach is to gain a very fast computing model and to get a benchmark for an advanced EC model. The EC consists of one element for every section of the ideal impedance spectrum of lithium-ion cells and is displayed in Fig. 2.

The impedance behaviour of the cell at very high frequencies is represented by an ideal inductor *L* and the ohmic resistance by a resistor *R*. The following electrochemical processes at the electrodes can be represented in a most simple way by RC-elements,

* Corresponding author. Tel.: +49 (0) 7021 89 2589; fax: +49 (0) 711 305214 2286.
E-mail address: dave.andre@daimler.com (D. Andre).

0378-7753/$ – see front matter © 2010 Elsevier B.V. All rights reserved.
doi:10.1016/j.jpowsour.2010.07.071

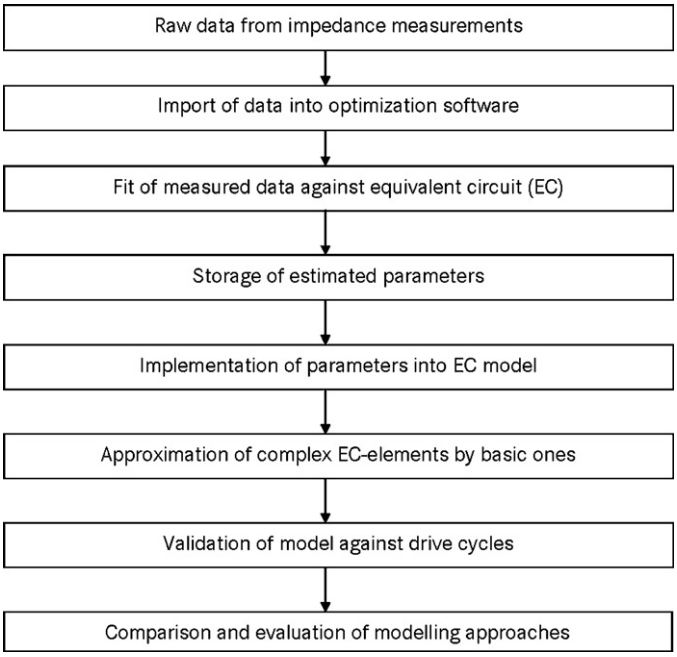

Fig. 1. Approach of system identification for an EC model.

a parallel connection of a capacitor C and a resistor R. Thus the impedance of the system can be described as the sum of its elements:

$$\underline{Z}_{RC} = j\omega L + R_1 + \frac{1}{1/R_2 + j\omega C_2} + \frac{1}{1/R_3 + j\omega C_3} + \frac{1}{1/R_4 + j\omega C_4}. \quad (1)$$

This approach is a state of the art EC [4–7] and has in total eight parameters which have to be estimated and fitted by an optimization algorithm.

2.2. Equivalent circuit with Zarc and Warburg element

The goal of the second EC is a most accurately and meaningful reproduction of the measured impedance data. An approach with Zarc and Warburg elements suggested by several authors [8–10] is shown in Fig. 3.

2.2.1. The Zarc element

Zarc elements are a parallel connection of a resistor R and a constant-phase-element (CPE) [11]. CPEs consist of a generalized

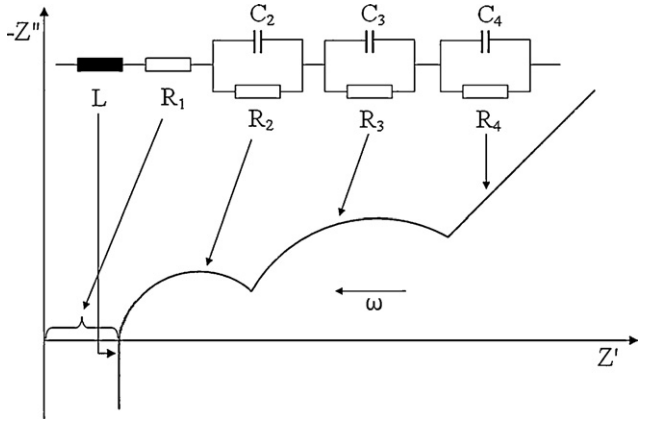

Fig. 2. Ideal impedance spectrum of a lithium-ion cell and an EC with three RC-elements.

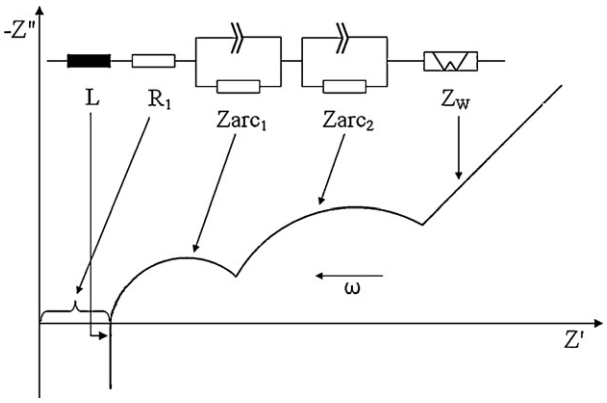

Fig. 3. Ideal impedance spectrum of a lithium-ion cell and an EC with Zarc and Warburg element.

capacity θ and depression factor ψ and are defined by

$$\underline{Z}_{CPE} = \frac{1}{(j\omega)^{\psi}\theta}. \quad (2)$$

A parallel connection with a resistor leads to Eq. (3):

$$\underline{Z}_{Zarc} = \frac{1}{1/R + (j\omega)^{\psi}\theta}. \quad (3)$$

Comparing Eq. (3) with the RC-element of Eq. (1) both equations are equal, if ψ is left aside.

This depression factor ψ, valid between zero and one, is responsible for the depression of the semi-circle in a Nyquist plot as Fig. 4 illustrates. For $\psi = 0$ the Zarc element represents only an ohmic resistance and for $\psi = 1$ the ideal semi-circle of a RC-element. The advantage of Zarc elements is their potential to reproduce the depression of semi-circles in impedance spectra, which are characteristic for lithium-ion cells. However, the disadvantage of Zarc elements is a missing Laplace transformation. Thus it is not possible to transfer the parameter sets from the frequency domain into the time domain without approximations [12].

Buller [13] introduced in his thesis a way to approximate Zarc elements by a variable number of RC-elements as illustrated in Fig. 5.

The principle of this approximation is based on an odd number of semi-circles whose radii are increasing towards the medium semi-circle. The resistance and capacity of each RC-element can be computed by optimization factors which are listed in the literature [13]. In Fig. 6, the result of an approximation with five RC-elements,

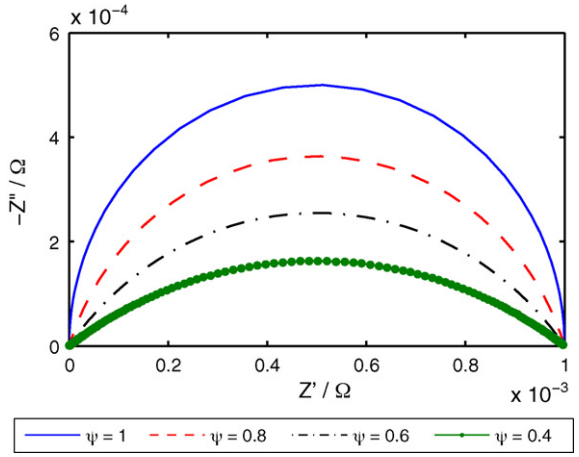

Fig. 4. Impact of depression factor ψ on the Nyquist plot of the Zarc element ($R = 1\ m\Omega$, $C = 1\ kF$).

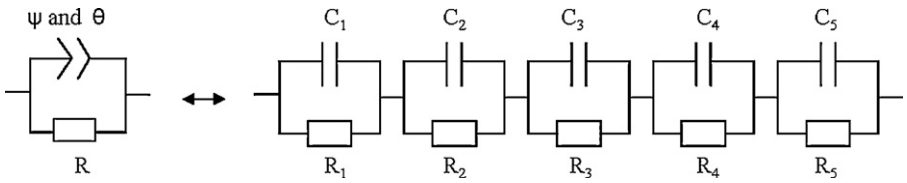

Fig. 5. Approximation of the Zarc element with five RC-elements.

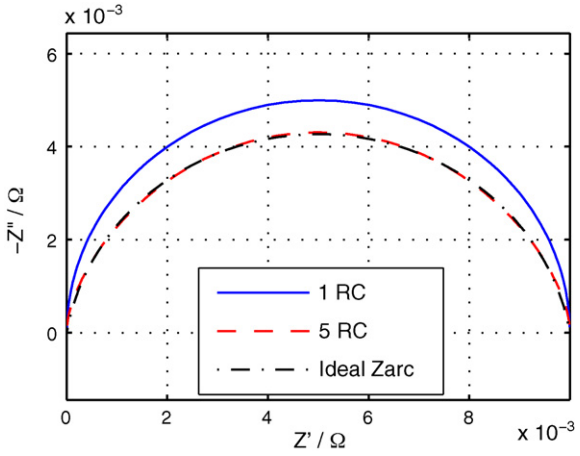

Fig. 6. Nyquist plot of a Zarc approximation with five RC-elements, the dash-dotted line represents the ideal Zarc element, the dashed line represents the circuit with five RC-elements and the solid line represents the circuit with just one RC-element ($R = 10\,\text{m}\Omega$, $C = 2\,\text{kF}$ and $\psi = 0.9$).

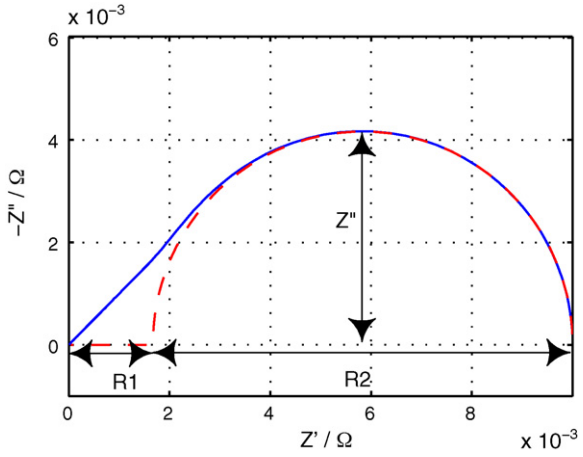

Fig. 7. Nyquist plot of Warburg element, the solid line represents the ideal Warburg element and the dashed line represents the R–RC circuit.

as used in this work, in comparison to an approximation with just one RC-element is shown.

Especially for high values of ψ the approximation matches the ideal curve very accurate and is therefore valid.

2.2.2. The Warburg element

Analogous to the Zarc element, an approximation is required for the Warburg element. A Warburg element is defined by

$$\underline{Z}_w = R\frac{\tanh(\sqrt{j\omega\theta})}{\sqrt{j\omega\theta}} \tag{4}$$

and shows a linear slope with an angle of 45° at high frequencies. This linear slope predestinates Warburg elements to represent the diffusion process of Fig. 3.

A simple way to approximate the Warburg element is a series connection of a resistor and a RC-element as illustrated in Fig. 7. An approach applied by Handschuh [14]. The impedance for this connection is

$$\underline{Z}_w = R_1 + \frac{1}{1/R_2 + j\omega C_2}. \tag{5}$$

For the estimation of the parameters R_1, R_2 and C_2, the frequency ω_0 where the spectrum reaches its minimum value is required. Handschuh [14] showed that the value of ω_0 is independent of R and can be approximated well by

$$\omega_0 = \frac{2.53}{\theta}. \tag{6}$$

Furthermore it was shown that the minimum value of the spectra depends only on the resistance

$$Z''_{\text{min}} = -\frac{5}{12}R. \tag{7}$$

By using this equation, the parameters can be determined:

$$R_1 = \frac{1}{6}R, \tag{8}$$

$$R_2 = \frac{5}{6}R, \tag{9}$$

$$C_2 = \frac{1}{\omega_0 R_2} = \frac{6}{5}\frac{1}{\omega_0 R}. \tag{10}$$

In order to get an approximated slope of 45°, R_1 has to be separated in additional two RC-elements with following parameters:

$$R_{1,1} = \frac{1}{24}R, \tag{11}$$

$$R_{1,2} = \frac{3}{24}R, \tag{12}$$

$$C_{1,1} = \frac{1}{100}C_2, \tag{13}$$

$$C_{1,2} = \frac{1}{3}C_2. \tag{14}$$

Finally, this approximation allows to representing the slope with high accuracy as demonstrated in Fig. 8.

Since for this work just the linear part of the Warburg element is required, the last approximation is done for the intersection of a tangent which runs through the point of origin and the RC-element by their geometrical relation:

$$R_3 = \frac{1-\sqrt{0.5}}{2}R_2, \tag{15}$$

$$C_3 = \frac{2}{2.42\cdot(1-\sqrt{0.5})}C_2. \tag{16}$$

By using these approximations it is possible to represent the Warburg element accurately. Thus the impedance of the advanced EC

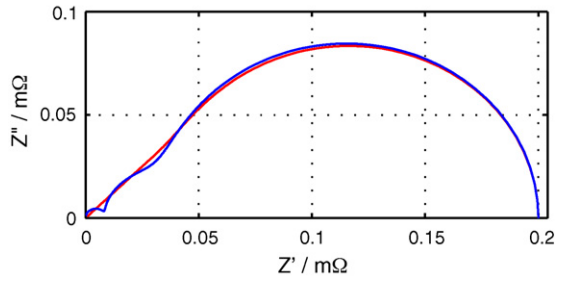

Fig. 8. Nyquist plot of a Warburg approximation with three RC-elements, the red line represents the ideal Warburg element and the blue line represents the 3-RC circuit. (For interpretation of the references to color in this figure legend, the reader is referred to the web version of the article.)

can be computed by the equation corresponding to Fig. 3:

$$\underline{Z}_{ZW} = j\omega L + R_1 + \frac{1}{1/R_2 + \theta_2 \cdot (j\omega)^{\psi_1}} + \frac{1}{1/R_3 + \theta_3 \cdot (j\omega)^{\psi_2}} + R\frac{\tanh(\sqrt{j\omega\theta_4})}{\sqrt{j\omega\theta_4}}. \quad (17)$$

In total this EC has ten parameters, two parameters more than the first EC, increasing the computation time but also the accuracy of the simulation.

3. Parameter estimation

3.1. Equivalent circuit with RC-elements

In this section, the parameters of the introduced ECs are estimated by numerical optimization. For this purpose a nonlinear curve-fitting optimization based on the method of least-squares was used for every spectrum. For in total 119 spectra, the parameters were estimated and interpolated to a characteristic map. Since for low temperatures no diffusion section was recorded by the electrochemical impedance spectroscopy (EIS) because of too low frequencies, an additional algorithm was required. This algorithm was able to detect the existence of a diffusion section in the measured data and was setting R_3 and C_3 to zero if no diffusion process was recorded.

The method of optimization is illustrated in Fig. 9 by plotting measured and fitted curves for an exemplary SOC of 60% at different temperatures in Nyquist plots. The general behaviour is similar for all temperatures. The simple EC is able to approximate the general behaviour of the curves, but fails to reproduce the spectra accurately. Problematic are the loops of the measured spectra which are depressed semi-circles and therefore difficult to fit by ideal ones and the almost linear diffusion part. Therefore large deviations can be seen especially in the middle of the first and second RC-element and for the linear slope at low frequencies. Since very high frequencies have no practical relevance for the simulation of batteries, the inductivity was neglected and is not represented.

3.2. Equivalent circuit with Zarc and Warburg element

The same optimization approach was applied to the second EC with Zarc and Warburg elements. The EC with estimated parameters was again compared to measured data and the result is given in Fig. 10.

It is obvious that this EC represents the measured data with a higher accuracy. Both, the semi-circles as well as the diffusion part are approximated very precisely by the Zarc and Warburg elements. Especially, the depressed semi-circles are represented very well by the depression factor ψ. However, small variations can still be seen for elevated temperatures at the change from the second Zarc element to the Warburg element.

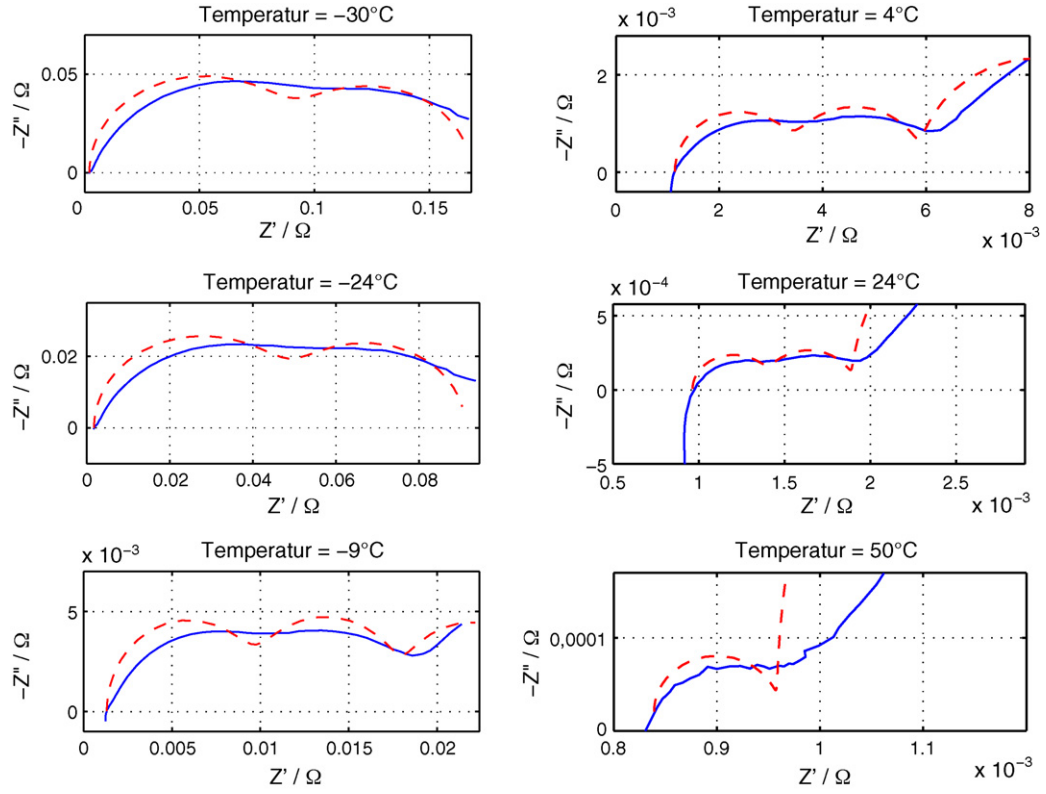

Fig. 9. Comparison of measured and simulated EIS data by the EC with RC-elements for different temperatures at 60% SOC, the solid line represents the measured spectra and the dashed line represents the simulated spectra.

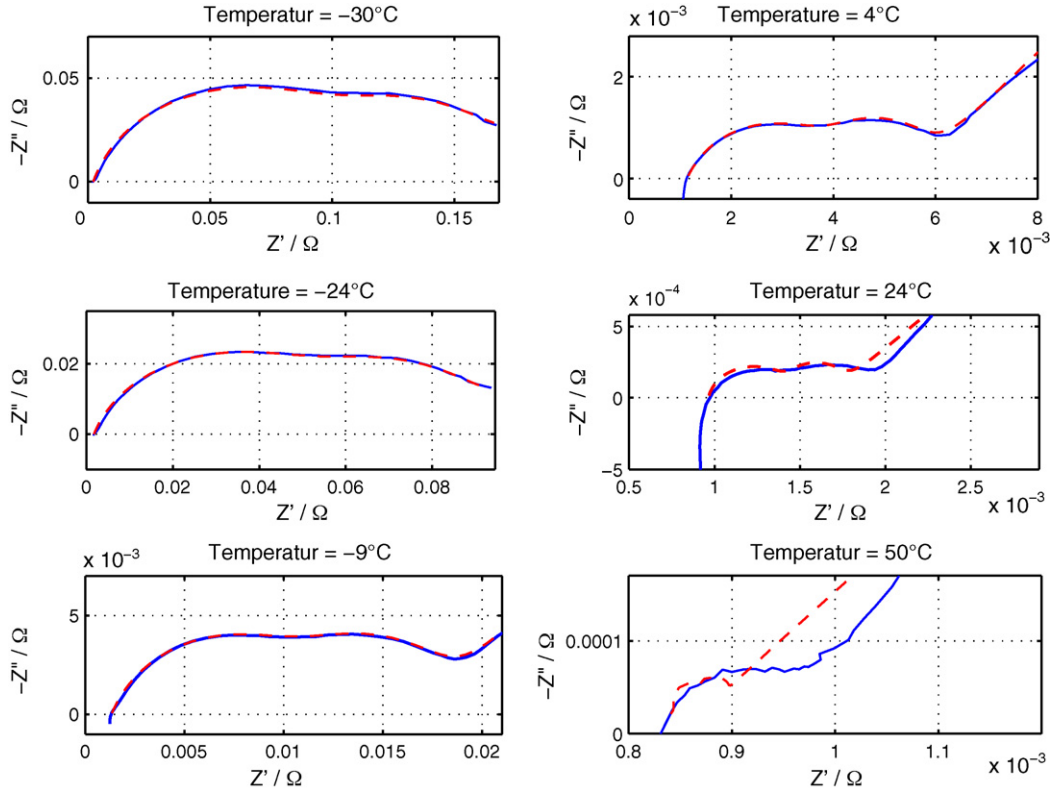

Fig. 10. Comparison of measured and simulated EIS data by the EC with Zarc and Warburg elements for different temperatures at 60% SOC, the solid line represents the measured spectra and the dashed line represents the simulated spectra.

4. Modelling

The estimated parameters were used to build cell models. Input parameters of this model were current I, cell capacity C, cell temperature T and initial state of charge $SOC_{t=0}$. By integrating the cell current, the actual SOC could be determined continuously. Furthermore the open-circuit voltage (OCV) curve of the cell, which was shown in [1], was approximated as a function of SOC by a lookup table. By adding the overvoltages η of the system, which are provided in form of the EC parameters, the actual cell voltage was computed and visualized.

4.1. Butler–Volmer adjustment

Since no DC-offset was used for the EIS measurements the effect of current on cell overvoltage was unknown. However, this effect is important for the charge transfer and is defined by the Butler–Volmer (BV) equation:

$$i = i_0 \cdot (e^{\alpha zF/RT(E-E_{eq})} - e^{-((1-\alpha)zF/RT)(E-E_{eq})}) \quad (18)$$

where i is the electrode current density, i_0 is the exchange current density, α is the symmetry factor, z is the number of electrons, E is the electrode potential, E_{eq} is the equilibrium potential, F is the Faraday constant, R is the universal gas constant and T is the temperature.

In order to consider the impact of current, a comparison was done between simulated (EC with RC-elements) and measured overvoltage for 18 s long pulses at 60% SOC at different temperatures. The differences between both curves were used to generate a lookup table with adjustment factors for the overvoltage as a function of temperature and current. Moreover it was observed that positive and negative current pulses cause very similar voltage responses. In consequence the symmetry factor α was set to 0.5.

4.2. Equivalent circuit with RC-elements

Three parts are necessary for modelling the actual cell voltage. The first one is a block for the calculation of the actual OCV. By integrating the current, the actual SOC is computed and recalculated in the open-circuit voltage by a lookup table. The second one, the ohmic resistance depending on the actual I, T and SOC is approximated by a lookup table. The last part is the overvoltages by the RC-elements.

For implementing the estimated parameters of the RC-element in the EC model, a correlation between input signal current I and output signal voltage U is required for every RC-element. The current of this parallel connection is:

$$I = I_R + I_C. \quad (19)$$

The current flowing through the resistor and capacitor are defined by

$$I_R = \frac{U}{R}, \quad (20)$$

$$I_C = C \cdot \frac{\partial U}{\partial t}. \quad (21)$$

Including Eqs. (20) and (21) in Eq. (19), the voltage of the RC-element can be calculated by

$$U = \int_{t=0}^{t=t_{end}} \frac{RI - U}{RC} \mathrm{d}t. \quad (22)$$

In this equation R and C are functions of SOC, T and are gained again by lookup tables. The current I is the time dependent input signal and the actual voltage can be calculated by numerical integration using Eq. (22). As introduced in Section 4.1 these impedances are corrected by determined BV parameters. Finally, the actual cell voltage is calculated by adding up all three voltages.

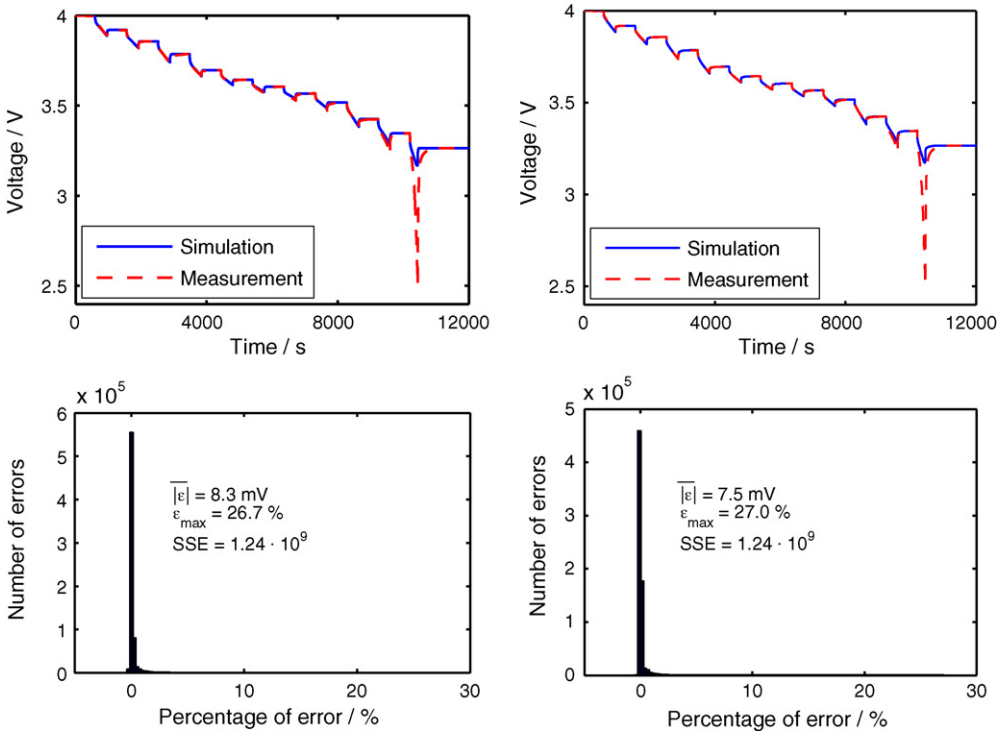

Fig. 11. Stepwise discharge, on top EC model with RC-elements, on bottom EC model with Zarc and Warburg elements.

4.3. Equivalent circuit with Zarc and Warburg element

The second modelling was done similarly to the described one. In addition, submodels based on the equations of Section 2.2 for the parameter estimation of the Zarc and Warburg approximations were built. Analogous to Fig. 11 the submodels were connected to a cell model and the actual cell voltage could be computed. Due to increased clarity in the further text, the cell model with RC-elements is abbreviated to RC model and the cell model with Zarc and Warburg element is abbreviated to ZW model.

5. Validation

Both models were validated against different current profiles in order to check their performance in a wide SOC and temperature range.

The first validation was carried out to test the models in the whole SOC range by comparing the results of cell characterization tests for simulation and measurement. Moreover, the models were tested and analysed for several cycling profiles and finally validated against data recorded during a hybrid electrical vehicle (HEV) drive.

Since the computation time plays an important role regarding applicability decisions, a summary of the computation times for all profiles is given in Table 1. The more complex ZW model with in total 13 RC-elements is by a factor up to four slower than the simple model with just three RC-elements.

Table 1
Comparison of computation times for different current profiles.

Profile	RC model (s)	ZW model (s)	Factor
Capacity test (~10,000 s)	97	179	1.8
Stepwise discharge (~12,000 s)	101	182	1.8
Test cycle $T = -20\,^{\circ}C$ (~6100 s)	40	96	2.4
Test cycle $T = 12\,^{\circ}C$ (~6100 s)	79	166	2.1
Test cycle $T = 50\,^{\circ}C$ (~6100 s)	58	231	4.0
HEV cycle (~2250 s)	41	105	2.6

However, for most profiles the computation time is just doubled and even for the more complex model the simulation time is always below 5% of the real time.

5.1. Stepwise discharge

The first validations were done for typical cell characterization tests such as cell charging and measurement of cell capacity. The result of the cell discharge in steps of 10% ΔSOC for measurement and simulation are shown in Fig. 12. It can be observed that both models were able to predict cell voltage with a high quality until a SOC of 10%. From 10% to 0% the cell voltage is dropping down, since the voltage reaches the end of discharge voltage limit. Both models are not able to simulate this phenomenon, since the Butler–Volmer coefficient α is probably varying at low SOC. In order to compare the results of both models, the mean value of the absolute error $\overline{|\varepsilon|}$, the maximum error ε_{max} as well as the sum of squared errors (SSE) between measured and simulated cell voltage are given in addition in all figures.

Both models show a similar distribution of voltage deviations and have a very comparable performance with a mean error of about 8 mV. No difference can be seen for the SSE, indicating the same quality of simulation for both models. Moreover a maximum error of 27% exists, but is occurring just for a negligible number of measurement points at very low SOC.

5.2. Test cycle

The next validations were done against drive cycles at five different temperatures measured in the laboratory. Only the results for 12 °C are shown which are representative for the observations at other temperatures. The test cycle consists of a mix of pulses, crankings and drive data for a period of 1.7 h. Fig. 13 shows the different grade of resolution for the comparison of simulation and measurement. Therefore in a second figure (Fig. 14) just a time slot of the first 20 min is shown.

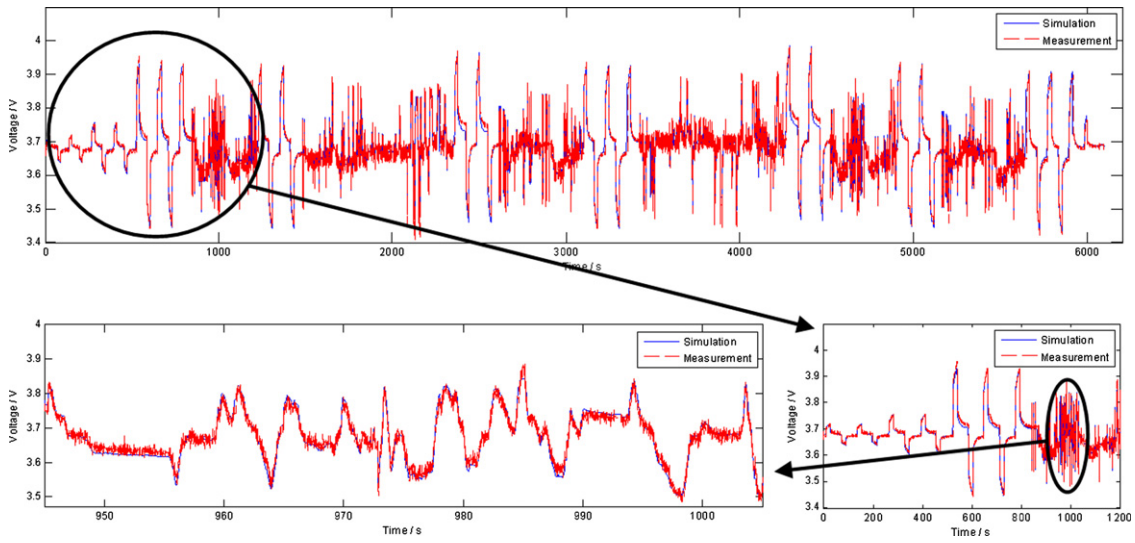

Fig. 12. Test cycle measurement and simulation.

Both models showed again a very satisfying agreement with the measured values. Especially, the zoom in Fig. 13 shows that even the simple model is able to represent fast voltage variations within few seconds very well. The error diagram shows very similar values and just a small improvement of SSE can be seen for the ZW model.

5.3. Drive cycle

The last profile was measured during test drives in South Africa and is very suited to test the models in consideration of high SOC variations (ΔSOC > 30%) and temperature variations.

By comparing the error distributions in Fig. 14 it is obvious that the RC model has a wider variation and almost doubled SSE compared to the ZW model. Moreover both models underestimate the cell voltage most of the time, especially at SOCs below 60% which is probably a consequence of the BV adjustment which is only valid for a SOC of 60%. Even if the voltage peaks are not simulated accurately, both models show in general a very good agreement with a mean error below 20 mV and predict therefore the cell performance very accurately.

A summary of the simulation quality represented by the mean error for all tests is given in Table 2. Except one case the more complex ZW model predicts the cell voltage with a higher accuracy. In

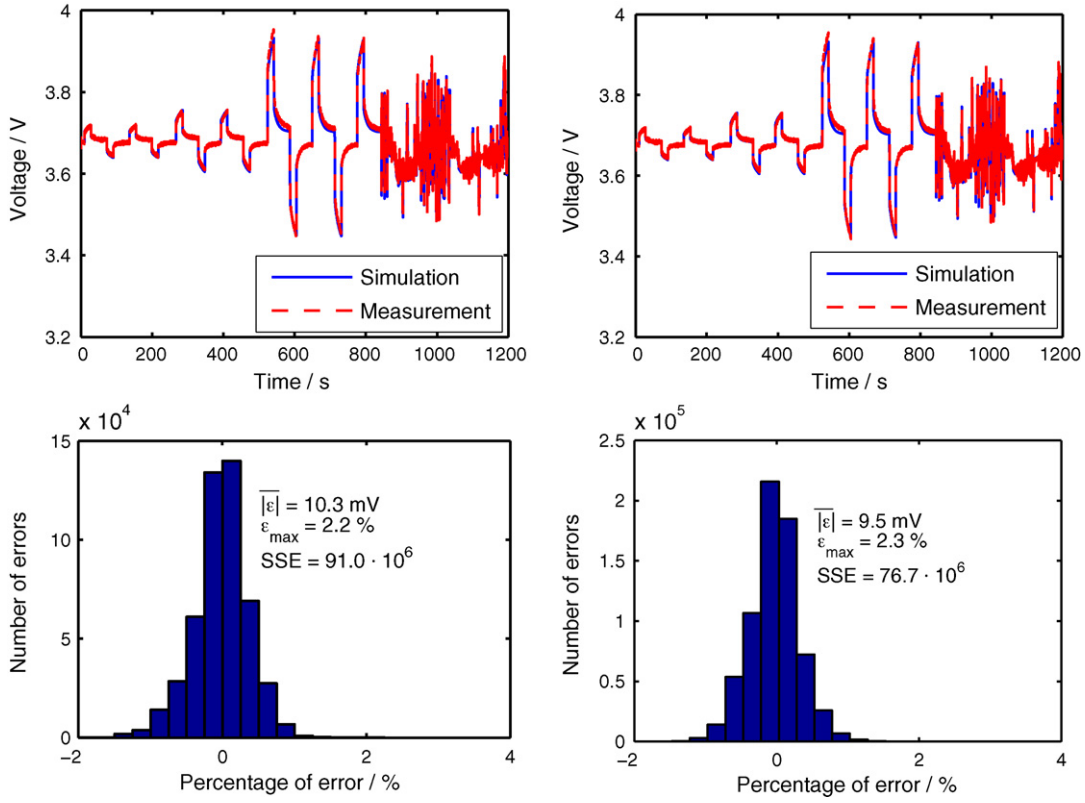

Fig. 13. Test cycle at $T = 12\,^{\circ}C$, on top EC model with RC-elements, on bottom EC model with Zarc and Warburg elements.

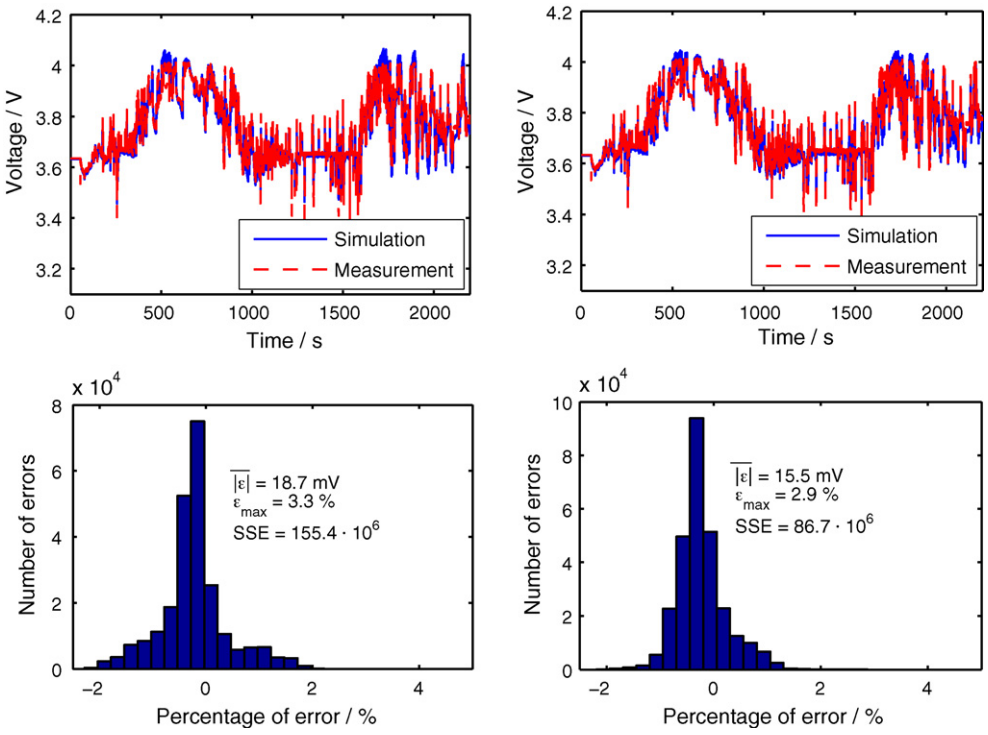

Fig. 14. Drive cycle, on top EC model with RC-elements, on bottom EC model with Zarc and Warburg elements.

Table 2
Comparison of voltage deviations for different current profiles.

Profile	RC model (mV)	ZW model (mV)	$\Delta\varepsilon$ (%)
Capacity test	11.1	10.5	5.4
Stepwise discharge	8.3	7.5	9.6
Stepwise charge	7.7	7.2	6.5
Test cycle $T = -20\,^{\circ}C$	10.6	10.6	0
Test cycle $T = -8\,^{\circ}C$	5.9	7.7	−30.5
Test cycle $T = 12\,^{\circ}C$	10.3	9.5	8.0
Test cycle $T = 30\,^{\circ}C$	8.3	6.7	19.3
Test cycle $T = 50\,^{\circ}C$	7.8	7.1	2.6
HEV cycle	18.7	15.5	17.1

general the improvement of simulation is in the range of 5–20%, but is always below 3 mV.

6. Results and discussion

In the last section, two different EC models were introduced. First, a simple model based on an EC of three RC-elements and second a more complex model based on Zarc and Warburg elements. The parameters of both ECs were estimated by a fitting for a large number of measured impedance spectra. It was shown that the simple EC was not able to reproduce the measured data even with optimized parameters sufficiently. In opposite, the more advanced EC was reproducing the spectra very accurate. Since for Zarc as well as Warburg elements no Laplace transformation exists, approximations were derived. These gained ECs were implemented in cell models. Afterwards both models were validated against different experimental data as cell characterization tests, test cycles and drive cycle.

All validations showed that both models predict cell voltage very precisely. Although the simple EC was not able to reproduce the impedance curves, voltage was predicted with a high quality. Comparisons of both models evidenced an up to 20% higher mean error for the simple model by a minimum doubled computation speed. However, also the mean error for this model is just in the range of a few mV. Therefore it can be concluded that the impedance fitting plays a role for the simulation quality, but the influence is just small and voltage can also be predicted accurately by simple EC models.

To sum up, both EC models allow a very precisely prediction of battery voltage and battery performance. Thus it is possible to use these battery models for simulations of e.g. consumption, vehicle range, cooling requirement and battery lifetime prognosis.

References

[1] C. Andrés, C.F. Valerio, P. Franz, Conference Paper 3rd European Ele-Drive Transportation Conference, Geneva, 2008.
[2] V.H. Johnson, A.A. Pesaran, T. Sack, Conference Paper 17th Annual Electric Vehicle Symposium, Montreal, 2000, http://www.nrel.gov/docs/fy01osti/28716.pdf.
[3] D. Andre, M. Meiler, K. Steiner, C. Wimmer, T. Soczka-Guth, D.U., Journal of Power Sources, submitted for publication.
[4] C.H. Chen, J. Liu, K. Amine, Journal of Power Sources 96 (2) (2001) 321–328, http://www.sciencedirect.com/science/article/B6TH1-42YW1MK-6/2/55c83acb31add2c5842027197de2d198.
[5] K. Xu, S. Zhang, R. Jow, Journal of Power Sources 143 (1–2) (2005) 197–202, http://www.sciencedirect.com/science/article/B6TH1-4F83PK6-6/2/1521fba1fc19b6471990df79e4999df9.
[6] S.R. Nelatury, P. Singh, Journal of Power Sources 132 (1–2) (2004) 309–314, http://www.sciencedirect.com/science/article/B6TH1-4C2FG3J-1/2/4a111ad6d7d3596cc6edf39c7ff04006.
[7] A. Jossen, Journal of Power Sources 154 (2) (2006) 530–538, http://www.sciencedirect.com/science/article/B6TH1-4HP6G8C-3/2/3f7544a06aa39abad3c51eee6e76f7cb.
[8] J. Gerschler, D.U. Sauer, EET-2007 European Ele-Drive Conference, Bruxelles, 2007.
[9] G. Ning, B. Haran, B.N. Popov, Journal of Power Sources 117 (2003) 160–169.
[10] J. Shim, K.A. Striebel, Journal of Power Sources 122 (2003) 188–194.
[11] E. Barsoukov, J.R. Macdonald (Eds.), Impedance Spectroscopy Theory, Experiment, and Applications, 2nd ed., John Wiley & Sons, 2005.
[12] A. Lasia, Electrochemical Impedance Spectroscopy and its Applications, Modern Aspects of Electrochemistry, vol. 32, Kluwer Academic/Plenum Publishers, New York, 1999.
[13] S. Buller, Impedance-based Simulation Models for Energy Storage Devices in Advanced Automotive Power Systems, Aachener Beiträge des ISEA, Band 31, Shaker Verlag GmbH, Aachen, 2003.
[14] T. Handschuh, Analysis of the operation and ageing behaviour of lead-acid batteries for typical stress conditions of hybrid electric propulsion systems, Ph.D. Thesis, University of Ulm, 2007. http://vts.uni-ulm.de/query/longview.meta.asp?document_id=5938.